DILUTION MONITORING FOR THE BDF/SHiP TARGET

D. Gancarcik*, D. Belohrad, A. Goldblatt, M. A. Fraser, D. Metin, L. J. Nevay,
M. M. Nieto, F. Roncarolo, CERN, Geneva, Switzerland

Abstract

The BDF/SHiP experiment requires precise monitoring of the beam dilution pattern on the high-power target absorbing up to 350 kW (avg.). This paper presents the conceptual design of a dedicated Beam Dilution Monitor (BDM), which will enable observation of the circular beam sweep pattern during 400 GeV/c proton operation. The proposed system is based on Secondary-Emission Monitor (SEM) grids comprising 12 µm-thick titanium bands. Detailed simulations were performed to evaluate signal formation, thermal response, secondary-electron collection, and the detectability of dilution magnet failure scenarios. Different detector geometries and interlock strategies were also investigated, demonstrating that the proposed BDM concept can provide sufficiently fast and reliable detection of dilution failures.

INTRODUCTION

The Beam Dump Facility (BDF) is a new, high-intensity facility to be installed in CERN's North Area (NA), developed to receive a high-intensity 400.3 GeV/c proton beam from the Super Proton Synchrotron [1, 2]. The facility will host the Search for Hidden Particles (SHiP) experiment, which aims to explore physics beyond the Standard Model by detecting feebly interacting and long-lived particles produced in proton–target interactions. The BDF relies on directing the proton beam onto a dense target to force interactions. Downstream, an extended hadron absorber and muon shielding system suppress the flux of secondary particles reaching a dedicated low-background decay volume. However, interactions of the primary beam with residual gas and beamline elements upstream of the target can generate a significant muon background that escapes the muon shielding system [3]. Although the beamline will operate under primary vacuum, strict constraints are placed on the amount and location of material introduced along the beamline. In particular, the necessary interceptive beam instrumentation must minimise the material introduced into the beam path and be positioned as close to the target as possible, so any muons created enter the acceptance of the muon shield.

Due to the high beam power on target, transverse dilution is required to limit the peak energy deposition. This is achieved using a system of two horizontal and two vertical magnets installed ~100 m upstream of the target, resulting in a circular sweep with a radius of 50 mm on target and completing four turns during the 1 s-long spill [4]. The nominal beam intensity and RMS beam size at the target is 4×10^{13} p$^+$ and 16 mm, respectively. Any deviation from the nominal sweep pattern can lead to a significant increase in local energy deposition, which poses a risk to the target. Leaving the beam undiluted for more than ~100 ms would result in damage to the dump and cause unwanted downtime [5].

A Beam Dilution Monitoring (BDM) system is therefore required to continuously verify the beam trajectory and trigger a beam abort in the event of a malfunction [2]. For machine protection purposes, the system must robustly detect deviations from the nominal sweep pattern with sufficient temporal resolution and low latency to identify dangerous conditions on timescales well below 100 ms. The expected annual operation of 10^6 spills requires high reliability and a very low false-abort rate. The BDM should also provide beam position and size measurements for beam optimisation and to be used by SHiP. Unlike the robust and low-latency machine protection functionality, these diagnostic measurements can rely on more advanced reconstruction and signal processing techniques since they are not part of the primary interlock chain.

BEAM DILUTION MONITOR DESIGN

Two identical BDM units will be produced, each consisting of two orthogonal SEM grids. The upstream and downstream units will be installed at 20 m and 10 m upstream of the target, respectively, corresponding to beam size and sweep radius reduction relative to the target location. To minimise the amount of material permanently present in the beam path, the upstream unit is designed to be retractable, while the same mechanical concept has been adopted for both BDM units for design uniformity. Using two BDM units also allows the beam trajectory angle to be reconstructed and provides redundancy for machine protection.

Several materials have been considered for the BDM bands. A recent beam test conducted in the NA evaluated the performance of different materials for beam profile monitoring under high-intensity conditions [6]. An unbunched 400.3 GeV/c proton beam with intensities of up to several 10^{13} p$^+$/spill was directed at wires made of various materials, with the beam impacting different transverse positions to assess their response. Among the tested candidates, titanium and tungsten showed good overall performance. However, the higher density of tungsten increases particle shower development, making titanium the selected baseline bans material. This beam test also demonstrated a linear response for approximately 0.05 to 2×10^{10} intercepted protons per band with Signal-to-Noise Ratio (SNR) above 13 using the CERN SEM Digital Acquisition System (DAQ).

The BDM's active area is defined to cover the full transverse beam excursion of ±50 mm, with an additional margin to account for the beam stay-clear region at the extremities of the sweep. The titanium bands, with a thickness of 12 µm

* david.gancarcik@cern.ch

in the beam direction, are well established in NA beam instrumentation through extensive operational experience. Although thinner foils could further reduce the material budget, they introduce increased challenges in terms of handling and mechanical stability. The baseline geometry employs bands of 3.5 mm width with a pitch of 6.5 mm. Relatively wide bands intercept a larger fraction of the beam, increasing the signal amplitude. A geometry with a constant pitch and 32 channels per plane was chosen in order to maintain a simple, robust detector layout while providing sufficient granularity for reliable sweep reconstruction and failure detection.

The impact of the proton beam on the bands was simulated using the FLUKA particle transport code [7]. The average energy deposition per primary proton was calculated to 0.4 MeV cm^{-3}. Assuming an adiabatic temperature rise and a full beam impact localized at a single position, the resulting temperature increase was estimated to be below 1 K per spill. The resulting temperature rise is therefore negligible for all considered operating conditions.

The signal will be sampled at 500 Hz, enabling synchronisation with the 50 Hz mains frequency, while still ensuring sufficient charge collection per sample for reliable signal detection. The proposed BDM DAQ consists of independent front-end and back-end systems for each monitor unit to minimise the risk of common failures. The front-end, located close to the monitors in a radiation-shielded area in the tunnel, performs analogue processing, digitisation of the 2×32 channels, motor control, and data transmission via an LpGBT [8] optical link. The back-end, located in a nearby service building, implements the LpGBT protocol and signal processing for beam reconstruction, machine protection, and timing distribution in the FPGA. Radiation studies [9] indicate annual doses below 1 kGy at 1 m from the beam axis for the downstream BDM unit, compatible with the proposed electronics architecture. Since the system is currently under development, the final implementation may evolve during the ongoing hardware R&D phase.

EXPECTED SIGNAL & REACTION TIME

The central 16 bands in each plane are directly intercepted by the beam during the sweep. Owing to the circular beam motion, the projected transverse velocity varies along the trajectory, reaching its maximum near the centre of the detector projection and decreasing towards the turning points at larger transverse displacements.

The simulated signal induced in each band is calculated by integrating the number of primary protons intercepted within the corresponding transverse region of the detector plane. To emulate the finite response time of the acquisition chain, the reconstructed signal is obtained by combining recent samples in a sliding window of recent samples using exponentially decaying weighting coefficients normalised to unity as shown in Fig. 1. This introduces a characteristic signal tail in the direction opposite to the beam motion, reflecting the finite integration time of the system. In the present study, a window of 50 samples and a characteristic

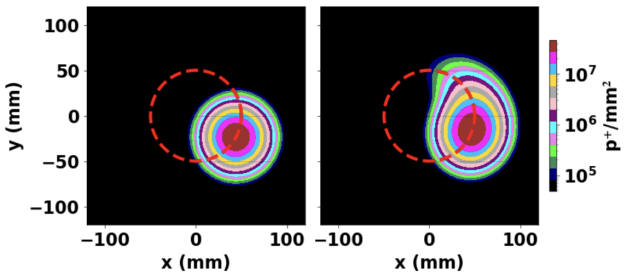

Figure 1: Ideal proton distribution (left) and one obtained by integrating over a sliding window of the 50 last samples using a characteristic decay time of 10 ms (right).

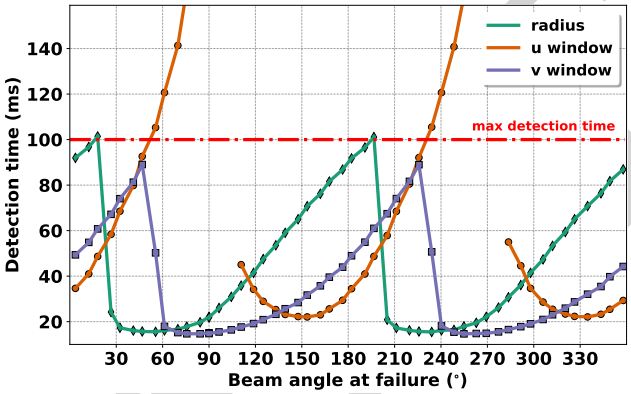

Figure 2: Detection time of a single horizontal magnet failure as a function of the beam angle at the moment of failure. Trigger algorithms based on: the reconstructed radius (green diamonds), position measured with grid in $u = 135°$-plane (orange circles), $v = 45°$-plane (purple squares) is shown.

decay time of 10 ms were assumed, corresponding to a conservative estimate of the acquisition response. Additionally, a SNR = 10 was assumed for the signal simulation.

Using the simulated signal, several interlock strategies are being investigated. A dynamic interlock window in each plane checks if the beam is at its expected position, assuming a fixed starting beam position during the spill. Additionally, by combining the position from both planes the radius of the motion is calculated and interlocked.

Under nominal conditions, the beam follows a circular trajectory, while failures of individual dilution magnets deform the sweep into an elliptical pattern with semi-minor axis aligned with the failure plane. The detection time depends strongly on the phase of the oscillation during the sweep. For SEM grids aligned with the same horizontal and vertical orientation as the dilution magnets, the failure in the horizontal plane is only measurable using the vertical grid, and vice versa. In contrast, rotated ±45° grids couple the motion across both detector planes, making the abnormal trajectory simultaneously visible in both planes. This is favourable for machine protection purposes. Figure 2 shows the detection time for the above-mentioned interlocks during the failure of a single horizontal dilution magnet. The detection time is periodic. The dynamic window and radial interlock can take up to 100 ms to register the failure because during the failure the beam trajectory initially remains close to the nominal

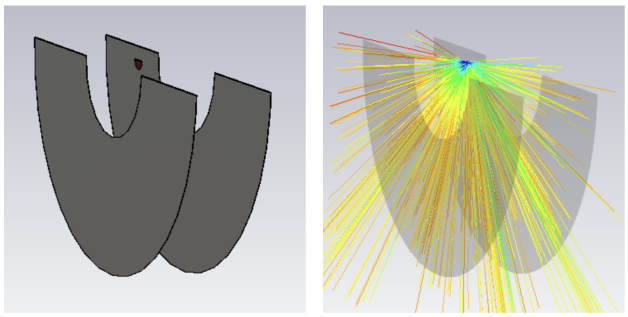

Figure 3: *Left:* CST model showing two anode rings (grey) at the distance of 6.4 cm from the SE source (red). *Right:* The simulated trajectory of SE for a bias voltage of 1 kV.

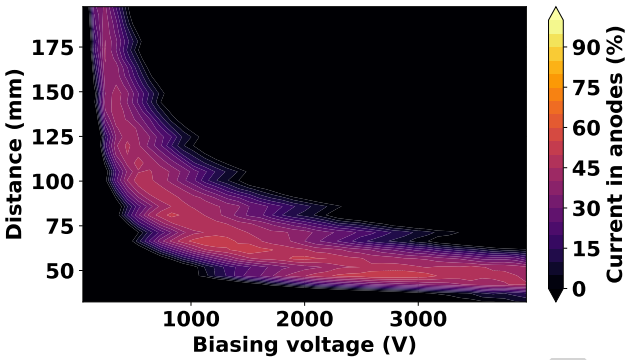

Figure 4: Fraction of SE collected by both anodes, as a function of the applied voltage and distance between anodes and the SEM grid, simulated with CST Particles Studio.

radius after the magnet failure and only gradually deviates from the circular sweep.

However, during this initial phase the beam still follows a near-nominal sweep pattern, such that the local energy deposition on the target remains relatively low despite the delayed detection. For failures of two magnets in the same plane, the detection times are significantly shorter and remain below approximately 30 ms. For three- and four-magnet failures, the maximum detection times are reduced to approximately 20 ms and 10 ms, respectively. The maximum detection time of the combined interlock strategy, obtained for the least severe failure case and based on the assumed signal integration window and decay time, remained below 60 ms. This suggest that BDM in this particular design will fulfil the machine protection requirements for the investigated scenarios. Furthermore, the results demonstrate that robust and fast failure detection requires the simultaneous operation of multiple interlock algorithms.

ELECTROSTATIC SHIELDING

Secondary electrons emitted from one band may be collected by a neighbouring band, degrading the SNR. To suppress this effect, an electric field is typically employed as foils interleaving the SEM grid. However, this configuration would induce particle showers and thus introduce additional background to the BDF. For this reason, equipping the SEM grid with an anode ring was investigated.

Less than 10^{-3} % of the primary beam, with a transverse centre at r=50 mm, intercepts an anode ring with an inner radius of 120 mm. Over the range from 120 mm to 160 mm, this fraction decreases by more than one order of magnitude for every 10 mm increase in radius.

Dedicated simulations using CST Particle Studio 3 were performed to determine the optimal distance between the grid and the anode ring (with hole radius between 120 mm to 160 mm) and optimal voltage bias of the anodes. Figure 3 illustrates the CST geometric model, which consists of a circular source centred at (x,y) = (50 mm, 0 mm) with a radius of 16 mm, emitting electrons towards the two collectors from both planes. The SE energy spectrum peaks at a few electron volts, and the emitted electrons follow an approximately cosine angular distribution with respect to the surface normal [11]. Accordingly, the electron energy was set to 10 eV with a spread of ±50 %, and the maximum angular emission was limited to 45°.

The trajectories of the secondary electrons were simulated and the fraction collected by the two anode rings was optimised. Figure 4 shows the percentage of SE collected by the anodes with a hole radius of 120 mm as a function of the distance between the source and the anode and of the applied voltage. The collected SE fraction increases with higher anode voltage and smaller grid–anode separation. The optimal distance between the anode and the SEM grid was found to be around 65 mm with each anode ring biased to 1.2 kV.

The impact of the anode hole size on the collection efficiency was also investigated for anode voltages in the range 1 kV to 1.4 kV. For an inner radius of 120 mm, the collection efficiency reaches approximately 54 ± 5 %, decreasing to 47 ± 5 % at 130 mm, 37 ± 5 % at 140 mm, 36 ± 5 % at 150 mm, and 31 ± 5 % at 160 mm. This demonstrates a clear reduction in collection efficiency with increasing hole size. However, the electrostatic field can worsen the signal of the SEM grid as the mobility of electrons and ions stemming from the beam-gas interaction differs [12].

SUMMARY AND OUTLOOK

A conceptual design of the BDM for the BDF/SHiP facility has been presented. The system is intended to provide continuous real-time monitoring of the transverse beam sweep during high-intensity proton operation while satisfying the strict material and background constraints imposed by the SHiP experiment. The proposed system consists of two SEM-based units using 12 µm-thick titanium bands with 3.5 mm width and 6.5 mm pitch sampled at 500 Hz. Simulations of dilution magnet failure scenarios demonstrated robust failure detection capabilities and showed that rotated ±45° grids improve redundancy and sensitivity to abnormal beam motion compared to conventional horizontal and vertical layouts. Electrostatic simulations furthermore demonstrated efficient secondary-electron collection using anode-ring geometries compatible with the BDF background constraints. Future work will focus on prototype development and optimisation of the interlock algorithms.

REFERENCES

[1] C. Ahdida *et al.* (Physics Beyond Colliders Collaboration), *SPS Beam Dump Facility – Comprehensive Design Study*, CERN Yellow Reports: Monographs, CERN, Geneva, 2020. doi:10.23731/CYRM-2020-002

[2] M.A. Fraser and C. Ahdida *et al.*, "The High Intensity ECN3 Project and the SPS Beam Dump Facility at CERN", presented at IPAC'26, Deauville, France, May 2026, paper THP4061, this conference.

[3] F. Stummer *et al.*, "Monte-Carlo Simulations of Beamline-Induced Muon Backgrounds for the SHiP Experiment" presented at IPAC'26, Deauville, France, May 2026, paper THP4070, this conference.

[4] A. Gorn *et al.*, "Machine protection considerations for transfer of the high-intensity proton beam to the BDF at CERN", presented at IPAC'26, Deauville, France, May 2026, paper WEP5049, this conference.

[5] M. Parkin *et al.*, "A Helium-Cooled Target Design at the SPS Beam Dump Facility (BDF) at CERN", presented at IPAC'26, Deauville, France, May 2026, paper THP4109, this conference.

[6] D. Metin *et al.*, "Performance of Titanium, Tungsten, and Carbon as Beam Profile Monitor Materials", in *Proceedings of the 14th International Beam Instrumentation Conference (IBIC 2025)*, Liverpool, UK, Sept. 2025, pp. 452–455. doi:10.18429/JACoW-IBIC2025-TUPMO03

[7] T.T. Böhlen, F. Cerutti, M.P.W. Chin, A. Fassò, A. Ferrari, P.G. Ortega, A. Mairani, P.R. Sala, G. Smirnov and V. Vlachoudis, "The FLUKA Code: Developments and Challenges for High Energy and Medical Applications", *Nuclear Data Sheets 120*, 211–214, 2014. doi:10.1016/j.nds.2014.07.049

[8] S. Biereigel *et al.*, "The lpGBT PLL and CDR Architecture, Performance and SEE Robustness", *PoS TWEPP2019*, 034, 2020. doi:10.22323/1.370.0034

[9] D. Wasik *et al.*, "Estimation of Radiation Field for BDF/SHiP at CERN", presented at IPAC'26, Deauville, France, May 2026, paper TUP8027, this conference.

[10] Dassault Systemes, *CST Studio Suite*, 2024.

[11] M. Taborelli, "Secondary Electron Yield of Surfaces: What We Know and What We Still Need to Know", *CERN Yellow Reports: Conference Proceedings*, vol. 3, p. 258, 2020. doi:10.4324/9781138609877-ree176-1

[12] Y. J. Lee, "Physics considerations for a harp system design at the Second Target Station of the Spallation Neutron Source", in *Proc. NAPAC'25*, Sacramento, California, USA, Aug. 2025, pp. 217–221. doi:10.18429/JACoW-NAPAC2025-MOP073